Applied Surface Science 509 (2020) 145246

Contents lists available at ScienceDirect

Applied Surface Science

journal homepage: www.elsevier.com/locate/apsusc

Full Length Article

# Effect of pre-adsorbed sulfur on $CH_x$($x$ = 1–3) formation from synthesis gas reaction over Cu(1 1 1) surface

Huan Lian[a], Hongyan Liu[a,b,*], Riguang Zhang[a], Lixia Ling[a,c], Baojun Wang[a,*]

[a] Key Laboratory of Coal Science and Technology of Ministry of Education and Shanxi Province, Taiyuan University of Technology, Taiyuan 030024, Shanxi, PR China
[b] College of Chemistry and Environmental Engineering, Shanxi Datong University, Datong 037009, Shanxi, PR China
[c] College of Chemistry and Chemical Engineering, Taiyuan University of Technology, Taiyuan 030024, Shanxi, PR China

ARTICLE INFO

*Keywords:*
Sulfur coverage
$CH_x$($x$=1–3) formation
Cu(1 1 1) surface
DFT

ABSTRACT

The presence of small amounts of sulfur in the syngas produced from fossil derived fuels is a major reason for deactivation of Cu-based catalysts. The formation of the key intermediates $CH_x$($x$ = 1–3) in the ethanol synthesis from syngas on sulfur covered Cu(1 1 1) surfaces is studied based on density functional theory. The results show that the adsorption energies of most surface species are heavily reduced after a sulfur atom pre-adsorbed on Cu (1 1 1) surface compared with clean Cu(1 1 1) except for CO, $CH_2O$ and CHOH, and the variation of the adsorption energies is not obvious with increasing sulfur coverage from 1/16 to 3/16 ML. When sulfur coverage is gradually increased, the adsorption energies of CO and CHOH have a downward and risen trend, respectively, while $CH_2O$ hardly changes due to its physical adsorption. The reaction activity of $CH_x$($x$ = 1–3) formation is seriously inhibited with sulfur added to the system. The presence of sulfur does not change the optimal reaction pathways and rate-limiting steps of CH formation, but changes the rate-limiting steps of $CH_2$ formation and the optimal reaction pathways of $CH_3$ formation. The dominant $CH_x$($x$ = 1–3) species are $CH_2$ and $CH_3$ at 1/16 ML sulfur coverage, and only $CH_3$ is the most favored $CH_x$($x$ = 1–3) monomer when increasing sulfur coverage up to 2/16 and 3/16 ML. Our results provide the detailed insight into the sulfur effect on the CH$x$($x$ = 1–3) formation on Cu surface.

## 1. Introduction

Synthesis gas is widely used to produce alcohol catalyzed by Co, Rh and Cu catalysts and the technology is mature and industrialized. Unfortunately, sulfur-containing compounds, especially hydrogen sulfide ($H_2S$), almost always present in synthesis gas from fossil energy [1], which seriously affect the reaction processes [2] and eventually cause irreversible deactivation or poisoning of metal catalysts.

In recent years, many researchers have paid more attention to the effect of sulfide in raw materials on metal catalysts encountered in the chemical reactions. Bitsch-Larsen and co-workers [3] studied the influence of $CH_3SH$ on the performance of catalytic partial oxidation (CPO) of $CH_4$ on Rh-Ce supported foam catalysts and suggested that the ppm levels of $CH_3SH$ lead to lower $CH_4$ conversion and lower $H_2$ selectivity. More importantly, increasing the $CH_3SH$ concentration from 14 to 28 ppm did not lead to significant changes about $CH_4$ conversion and $H_2$ selectivity, indicated that the poisoning effect was saturated at several ppm. Cimino and Lisi [4] studied the effect of sulfur poisoning during the CPO of $CH_4$ on Rh-based catalysts, and found that $CH_4$ conversion and $H_2$ selectivity both were progressively inhibited with $H_2S$ (8, 18 and 37 ppm) added to the feed, whereas the CO selectivity was almost impervious of $H_2S$ concentration. Legras et al. [5] studied the deactivation mechanisms of Ni/γ-$Al_2O_3$ catalysts for $CH_4$ synthesis from syngas containing small amounts of $H_2S$. At sulfur adsorption of 13.3, 48.1 and 131.0 μmol·$g^{-1}$, the decrease in CO hydrogenation rate was almost proportional to the sulfur adsorbed on the catalyst. Thus, it can be clearly seen that the feed containing small amounts of sulfide has different influence on the reaction, and some scholars think that the effect of sulfide on the reaction is linearly related to the content of sulfide, while others think that the reaction has no significant changes with the increase of sulfide content. But agreements have been reached that sulfide could be dissociated into atomic sulfur under reaction conditions, and then adsorbed on the catalyst surface, which hindered the adsorption of reactant molecules resulting in reducing active region for the reaction [6,7].

It has been investigated for the adsorption and decomposition of $H_2S$ on Fe(1 0 0) [8], Cu(1 0 0) [9], Cu(1 1 0) [10], Cu(1 1 1) [11–13], Pd(1 1 1) [13–15] and Ni(1 1 1) [11,13] surfaces through first principle

* Corresponding authors at: No. 79 Yingze West Street, Taiyuan 030024, China.
*E-mail addresses:* liuhongyan@tyut.edu.cn (H. Liu), wangbaojun@tyut.edu.cn (B. Wang).

https://doi.org/10.1016/j.apsusc.2020.145246
Received 28 August 2019; Received in revised form 4 December 2019; Accepted 1 January 2020
Available online 03 January 2020
0169-4332/ 

calculation. The results showed that $H_2S$ can be dissociated easily on metal surfaces. Moreover, the product of atomic sulfur adsorbed on Cu (1 1 1) surface had been affirmed in experimental and theoretical studies. The new Cu-S phase diagram based on the density functional theory (DFT) showed that decreasing the $P_{H_2}/P_{H_2S}$ ratio could result in that sulfur adsorption on Cu surfaces was thermodynamically favorable [16]. Face-center-cubic and four fold hollow sites were the most equilibrium sites for single sulfur atom adsorption on Cu(1 1 1) and Cu (0 0 1) surfaces, respectively. Meanwhile, atomic sulfur could bind strongly with the metal surface to prevent or modify further adsorption of reactant molecules [5,17–19]. Furthermore, the effect of sulfur coverage on the interaction between atomic sulfur and metal surface has been reported in many literatures. For example, the adsorption energy of sulfur atom generally increased with increasing sulfur coverage on Au(1 1 1) [20] and Co(0 0 0 1) [21] surfaces. On the contrary, the adsorption energy has a decreasing tendency on Fe(1 1 0) [22], Pt (1 1 1) [23] and Pd(1 1 1) [15,24] surfaces. As pointed out by May and co-workers [25], the interaction of sulfur atom with Cu(1 1 1) was strong, but the variation of the adsorption energy with respect to sulfur coverage could not show any regular.

Nowadays, the study of ethanol synthesis from syngas has become a research hotspot in the reaction system on Cu-based catalysts [26–28]. But $H_2S$ is one of the major impurities in syngas and a severe poison for metal catalysts, for example, $Cu/ZnO/Al_2O_3$ catalysts for methanol synthesis from syngas could not tolerate $H_2S$ over 0.1 ppm [29]. For ethanol synthesis from syngas, the recognized mechanism is involved two key issues: the formation of $CH_x(x = 1–3)$ hydrocarbon [30–32] and $C_2$ oxygenates of ethanol precursor [26,33,34]. In short, the mechanism of $CH_x(x = 1–3)$ formation on Cu-based catalysts is that $CH_xO$ ($x = 1–3$) or $CH_xOH(x = 1, 2)$ species are formed from CO hydrogenation and then followed by its dissociation, or the direct dissociation of CO followed by hydrogenation.

However, up to now, little information has been reported on the effect of sulfur coverage for $CH_x(x = 1–3)$ formation on Cu(1 1 1) surface. In order to obtain a series of conclusions about the effect of $CH_x(x = 1–3)$ formation after occupying the adsorption site by sulfur atom. In this work, it is investigated that the mechanism of the formation of $CH_x(x = 1–3)$ monomer at different sulfur coverage on Cu (1 1 1) surface, our aim is to illustrate the effect of sulfur on the $CH_x(x = 1–3)$ formation.

## 2. Computational details

### 2.1. Calculation methods

All calculations were carried out by using the Dmol$^3$ program in Materials Studio 8.0 [35,36]. The exchange-correlation energy was calculated by using the generalized gradient approximation with the Perdew-Burke-Ernzerhof functional (GGA-PBE) [37,38]. The effective core potential (ECP) method was applied for Cu atoms [39], while other atoms were treated with an all-electron basis set. The double-numerical basis set with polarization functions (DNP) was selected to expand the valence electron functions [40]. A Methfessel-Paxton smearing of 0.005 Ha and a Monkhorst-Pack grid of 3 × 3 × 1 have been performed. The transition states were searched by using the complete LST/QST method to determine accurate activation barriers of the elementary reactions [41].

For surface species adsorbed on sulfur covered Cu(1 1 1) surface, the adsorption energy ($E_{ads}$) was calculated as follows

$$E_{ads} = E_{sulfur+slab} + E_{species} - E_{species+sulfur+slab}$$

where $E_{species+sulfur+slab}$ is the total energy of the relaxed species and sulfur co-adsorbed on metal surface, while $E_{sulfur+slab}$ and $E_{species}$ are the total energy of sulfur covered metal surface and free surface species alone, respectively.

The activation barrier ($E_a$) and reaction energy ($\Delta H$) for the elementary reaction occurring on sulfur covered Cu(1 1 1) surface were calculated as follows

$$E_a = E_{TS+sulfur+slab} - E_{reactant+sulfur+slab}$$

$$\Delta H = E_{product+sulfur+slab} - E_{reactant+sulfur+slab}$$

where $E_{reactant+sulfur+slab}$, $E_{TS+sulfur+slab}$ and $E_{product+sulfur+slab}$ are the total energy of reactant, transition state and product on sulfur covered Cu(1 1 1) surface, respectively.

### 2.2. Surface models

The face-center-cubic Cu unit cell was optimized, and the calculated lattice constant of 3.61 Å is in accordance with the experimental value of 3.62 Å [42]. A three-layer slab was used to represent Cu(1 1 1) surface in this work which was always chosen in DFT calculations and the credible results could obtain based on the model [12,43–45]. A $p$ (4 × 4) supercell was applied where there are sixteen atoms at each layer, which corresponding to 1/16 ML coverage. Meanwhile, a vacuum region of 15 Å was employed to ensure no significant interaction between the periodically repeated slabs. In all calculations, the atoms in the upper two layers were allowed to relax with sulfur atoms and adsorbed species, whereas the bottom layer was kept frozen at the bulk position.

For the $p(4 \times 4)$ supercell, one, two and three sulfur atoms were adsorbed on clean Cu(1 1 1) surface to model the different surface sulfur coverage ($\theta_S$) of 1/16, 2/16 and 3/16 ML, respectively. The same method was employed in the previous DFT calculation to investigate the adsorption of atomic sulfur on Fe(1 1 0) surface [22]. Indeed, the coverage of 1/9, 1/4 and 1/2 ML can also be selected on Cu(1 1 1). However, at higher sulfur coverage, the products may be influenced by the surface coverage because of the relative short distance between the co-adsorbed species [46]. Moreover, the structural parameters such as atomic distances from the adsorbed sulfur to the surface of the catalyst show an almost constant value at 1/4 ML coverage [25]. More importantly, the extremely trace sulfur in syngas leading to the deactivation of Cu catalysts is the basis that we select sulfur coverage as low as possible to simulate the initial situation of sulfur poisoning. At the same time, computation efficiency and the size of the model also have to be considered during the investigation. Therefore, based on the above reasons, we chose the coverage of 1/16, 2/16 and 3/16 ML to study the effect of pre-adsorbed sulfur on $CH_x(x = 1–3)$ formation over Cu(1 1 1) surface.

Due to the importance of steric interactions between the neighboring atoms adsorbed on the surface, the most stably feasible surface structures of different sulfur coverage were determined. Fig. 1 displays the structures of Cu(1 1 1) surfaces at different sulfur coverage and the adsorption sites are labeled. It is the most stable site for sulfur atom over fcc site on clean Cu(1 1 1) surface and the corresponding adsorption energy is 431.5 kJ·mol$^{-1}$ which consists with previous DFT results [13,16,25,47]. Potential adsorption sites around sulfur atom are considered. There are ten possible adsorption sites for sulfur coverage of 1/16 ML (see Fig. 1(a)), and the most stable adsorption site for the second sulfur atom is occupying the F2 site with an adsorption energy of 427.4 kJ·mol$^{-1}$. After adsorption of two sulfur atoms on clean Cu (1 1 1) surface, $\theta_S$ = 2/16 ML (seen in Fig. 1(b)), the surface displays eight possible adsorption sites for other adsorbates. The best configuration for the third sulfur atom appears to occupy the F2 site with an adsorption energy of 421.9 kJ·mol$^{-1}$. Similarly, sulfur coverage of 3/16 ML reveals twelve possible adsorption sites for other adsorbates (seen in Fig. 1(c)). For sulfur atom adsorption at different sulfur coverage, the adsorption energies are found to be decreased with the increase of sulfur coverage, which is in accordance with previous results on Pd(1 1 1) [15] and Pt(1 1 1) [23] surfaces.

In addition, the attractive S-S interaction would cause to the formation of $S_2$ on the Au(1 1 1) at high sulfur coverage [20], but such

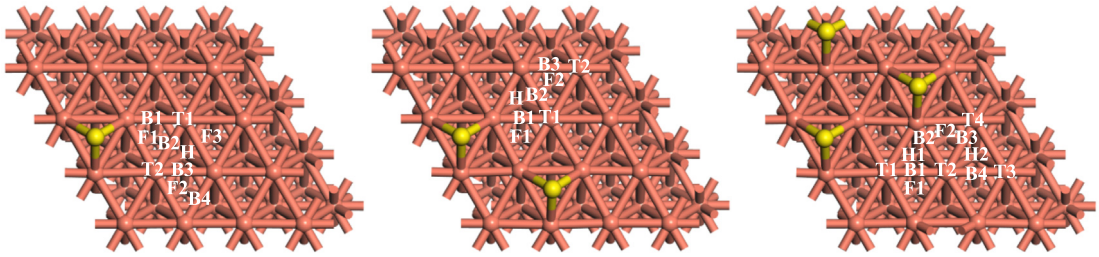


(a) $\theta_S$ = 1/16 ML (b) $\theta_S$ = 2/16 ML (c) $\theta_S$ = 3/16 ML

**Fig. 1.** Top view of sulfur covered Cu(1 1 1) surfaces and potential adsorption sites around sulfur atom. T, B, H and F refer to top, bridge, hcp and fcc sites, respectively.

phenomenon was not observed in the present work. Optimized the geometrical structure of $S_2$ adsorption on Cu(1 1 1) surface to check the stability of $S_2$/Cu(1 1 1) system, the desorption of $S_2$ was observed on Cu(1 1 1) surface, indicating that atomic sulfur is more stable than $S_2$ species at lower coverage. Hence, in this work, the formation of $S_2$ species was not considered on Cu(1 1 1) surface.

## 3. Results and discussion

### 3.1. Adsorption of all the possible species

The formation of $CH_x$($x$ = 1–3) from CO hydrogenation involves many elementary reactions. The reactants are CO and $H_2$ (here considering CO and H as the reactants), and the products are $CH_x$($x$ = 1–3). The intermediates are related to CHO, CHOH, $CH_2O$, $CH_2OH$ and $CH_3O$ according to previous reports [30–32]. Firstly, the adsorptions of all above species were investigated. As presented in Fig. 2, only the most stable adsorption structures for those species on Cu (1 1 1) surfaces with pre-adsorbed sulfur are provided with the calculated adsorption energies. Fig. 3 presents the variation of adsorption energies of all surface species at different sulfur coverage compared with our previous results on clean Cu(1 1 1) [30].

***CO, H, O and OH adsorption.*** The bond length of gas-phase CO was calculated to be 1.143 Å. CO was found to preferentially bind to the F2, F2 and H2 sites at 1/16, 2/16 and 3/16 ML sulfur coverage, respectively. The adsorption energies become a bit smaller compared with our previous result on clean Cu(1 1 1) surface [30]. Moreover, with the increase of sulfur coverage from 1/16 to 3/16 ML, the adsorption energies decrease which consists with the previous DFT results that the presence of sulfur weakens the bonding of CO to the Co(0001) [19], Fe (1 0 0) [48] and Pd(1 1 1) [49] surfaces. It is noteworthy that the C—O bond is stretched compared to gas-phase CO (1.182, 1.181 and 1.173 Å for 1/16, 2/16 and 3/16 ML sulfur coverage versus 1.18 Å on clean Cu (1 1 1) surface [30]). For H atom, it prefers to occupy the F2 and F2 sites at 1/16 and 2/16 ML sulfur coverage and adsorb at the H2 site when increasing sulfur coverage up to 3/16 ML. The adsorption energies of H atom heavily reduced after sulfur pre-adsorbed on Cu(1 1 1) compared to that on clean surface. However, the change of the adsorption energies is little when the sulfur coverage is increased from 1/16 to 3/16 ML. The favorable adsorption sites of O atom at different sulfur coverage which are found to be F2, F2 and F2 sites. Similar to the adsorption of H atom, the calculated adsorption energies of O atom are much weaker on sulfur occupied surface than that on clean surface. In addition, there is a decline with the increasing of sulfur coverage form 1/16 to 3/16 ML. The most stable sites of OH are the same as that of the H atom at different sulfur coverage. And the corresponding adsorption energies are heavily reduced compared those on clean Cu(1 1 1). Furthermore, the change of the adsorption energies is almost not apparent no matter what the sulfur coverage is.

***$CH_xO$($x$ = 1–3) adsorption.*** CHO prefers to adsorb at the T2 site at 1/16 ML sulfur coverage, and adsorb at the T1-B3 and T4-B4 sites at 2/16 and 3/16 ML sulfur coverage. The variation of adsorption energies of CHO is consistent with that of O atom. For the adsorption of $CH_2O$, it is physisorbed on the Cu(1 1 1) surface, therefore, it has little effect on its adsorption no matter which site it is adsorbed when sulfur covered on the catalyst. For $CH_3O$ adsorption on sulfur covered Cu(1 1 1) surfaces, the most favorable adsorption state is the structure with the O atom occupying the F2, F2 and H2 sites at 1/16, 2/16 and 3/16 ML sulfur coverage, respectively. The adsorption energies of $CH_3O$ is reduced after sulfur pre-adsorbed on Cu(1 1 1) compared to that on clean surface. But there is a slight rise with the increasing of sulfur coverage.

***$CH_xOH$($x$ = 0–2) adsorption.*** Only the sites where COH occupies the F2 sites are stable at sulfur coverage of 1/16 and 2/16 ML, and COH prefers to adsorb at the H2 site when increasing sulfur coverage up to 3/16 ML. The adsorption energies of COH have an apparent decrease when sulfur occupied the Cu(1 1 1) surface and they are also decreased accompanied the sulfur coverage increasing. For CHOH adsorption on sulfur covered Cu(1 1 1) surfaces, the most stable adsorption sites are the B4, B3 and T3 sites at 1/16, 2/16 and 3/16 ML sulfur coverage, respectively, indicating that pre-adsorbed sulfur atom affects the site preference of CHOH. It is worth noting that an abnormal phenomenon appears about the adsorption energies of CHOH. They are not decreased but increased with sulfur coverage increasing from 1/16 to 3/16 ML. In the case of $CH_2OH$, the most stable adsorption sites are the B3, T2-B2 and T3 sites at 1/16, 2/16 and 3/16 ML sulfur coverage, respectively. The adsorption energies are reduced compared that on clean Cu(1 1 1). It is noted that the adsorption energy of $CH_2OH$ is increased at 3/16 ML sulfur coverage compared those at 1/16 and 2/16 ML. This may cause by the lateral interaction between $CH_2OH$ and sulfur atoms.

***$CH_x$($x$ = 0–3) adsorption.*** The single C atom prefers adsorb at the F2 sites at 1/16 and 2/16 ML sulfur coverage and the B3 site at 3/16 ML. The single C atom adsorption energy is substantially reduced upon sulfur being pre-adsorbed on Cu(1 1 1) surface compared that on pure Cu(1 1 1). It is obvious that the pre-adsorbed sulfur has seriously weakened the adsorption of C compared to that on clean surface. Similar with the adsorption of CO, CH is also adsorbed at the F2, F2 and H2 sites at sulfur coverage of 1/16, 2/16 and 3/16 ML, respectively. The most stable sites of $CH_2$ are the F3, F2 and F2 on sulfur covered Cu (1 1 1) surfaces. Meanwhile, the variation of adsorption energies of $CH_2$ is consistent with that of CH. After considering various adsorption sites, $CH_3$ is observed at the F2 and F2 sites at sulfur coverage of 1/16 and 2/16 ML. It prefers to adsorb at the H2 site at sulfur coverage of 3/16 ML and the adsorption is strengthened compared the two former.

Generally speaking, the presence of sulfur usually hinders the adsorption of other adsorbates on the catalyst surface, and its ability to adsorption has been weakened with the increase of sulfur coverage [48]. From Fig. 3, it can be clearly seen that the adsorption energies of most surface species heavily are reduced after a sulfur atom pre-adsorbed on Cu(1 1 1) surface compared to those on clean surface, except CO, $CH_2O$ and CHOH. In addition, it only has a slight decrease in the adsorption energy of CO. It has little effect on the adsorption of $CH_2O$ because of its physical adsorption. Interestingly enough, the adsorption

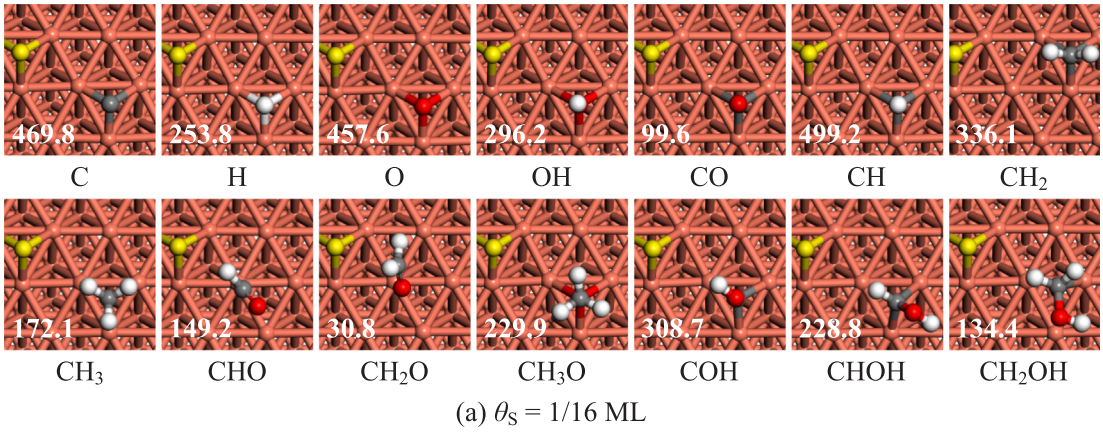


(a) $\theta_S$ = 1/16 ML

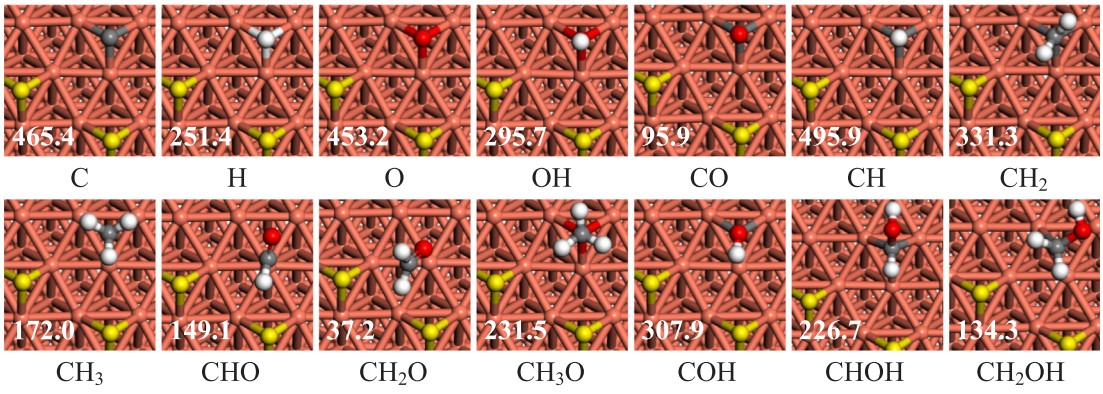


(b) $\theta_S$ = 2/16 ML

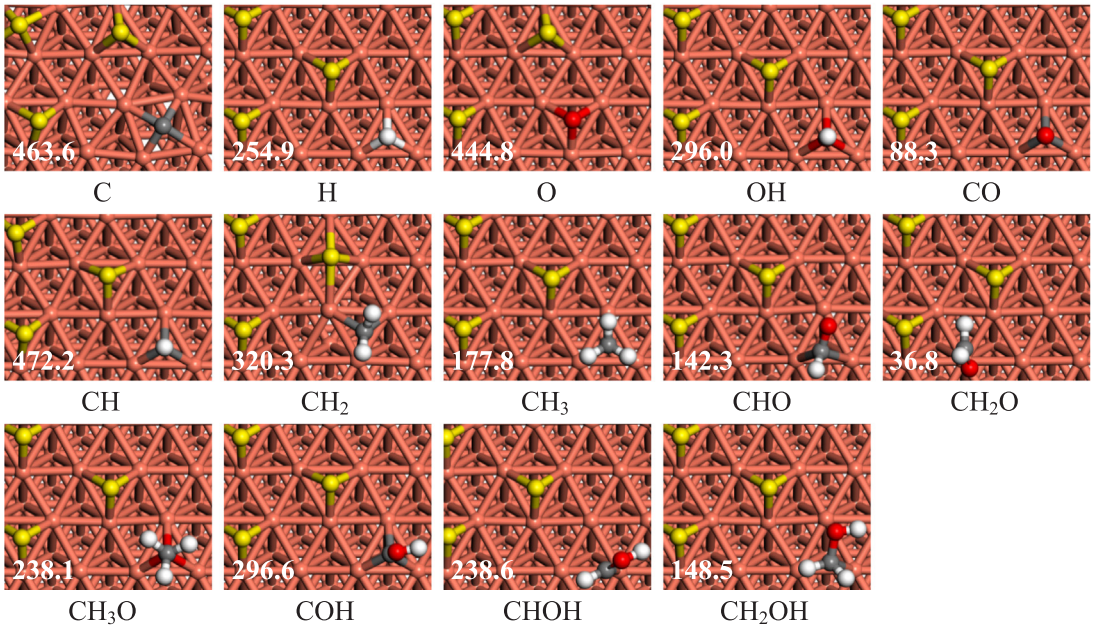


(c) $\theta_S$ = 3/16 ML

**Fig. 2.** The most stable adsorption sites of all surface species involved in $CH_x$($x$ = 1–3) formation at (a) 1/16 ML, (b) 2/16 ML and (c) 3/16 ML sulfur coverage. The adsorption energies (Unit: kJ·mol$^{-1}$) of all surface species are labeled on the bottom left of the pictures. Atomic color code: orange, copper; yellow, sulfur; gray, carbon; red, oxygen; and white, hydrogen. (For interpretation of the references to color in this figure legend, the reader is referred to the web version of this article.)

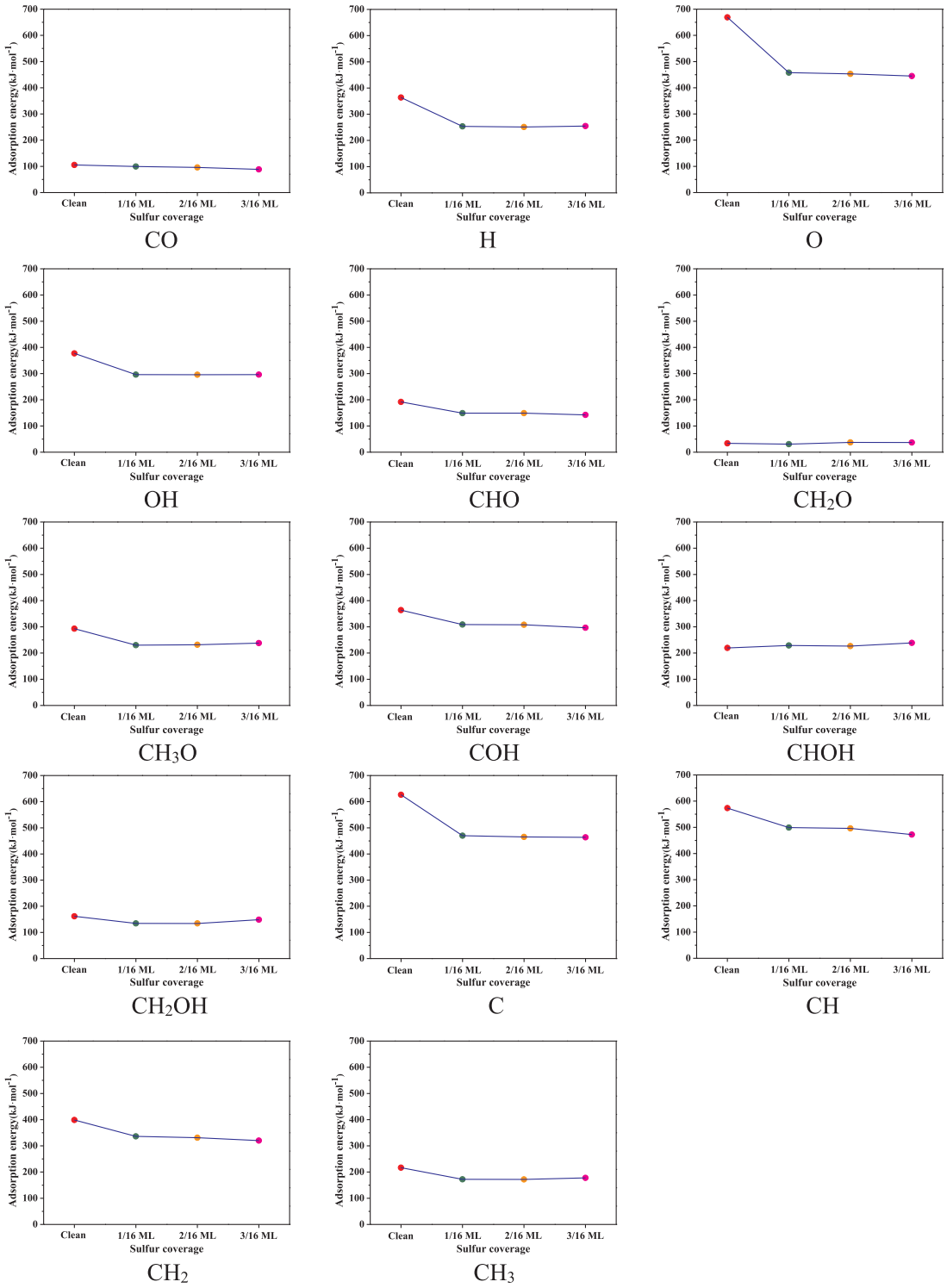


**Fig. 3.** The variation of adsorption energies for all surface species involved in $CH_x(x = 1–3)$ formation at different sulfur coverage.

energies of CHOH show a slightly increasing trend. The change of adsorption energies is little or almost unchanged when the sulfur coverage increases from 1/16 to 3/16 ML.

### 3.2. Formation of $CH_x(x = 1–3)$

The most dominant reaction steps for $CH_x(x = 1–3)$ formation are listed in Table 1, which were investigated in our previous work [30]. Herein, those steps are discussed again to clarify the influence of sulfur coverage on $CH_x(x = 1–3)$ formation. The corresponding activation barriers and reaction energies are also listed in Table 1.

#### 3.2.1. CO dissociation and hydrogenation

Starting from the adsorbed CO species, its direct dissociation and hydrogenation to form CHO or COH [30,34] are two activation ways responsible for the formation of $CH_x(x = 1–3)$ species. The transition states and activation barriers involved in CO dissociation and hydrogenation are provided in Fig. 4(a) and Table 1, respectively. The detailed potential energy profiles are shown in Fig. S1.

The activation barriers of CO direct dissociation on sulfur covered

**Table 1**
The activation barriers ($E_a$/kJ·mol$^{-1}$) and reaction energies ($\Delta H$/kJ·mol$^{-1}$) for the elementary reactions involved in $CH_x$($x$ = 1–3) formation at different sulfur coverage ($\theta_S$).

| Elementary reactions | | Clean[a] | | $\theta_S$ = 1/16 ML | | $\theta_S$ = 2/16 ML | | $\theta_S$ = 3/16 ML | |
|---|---|---|---|---|---|---|---|---|---|
| | | $E_a$ | $\Delta H$ | $E_a$ | $\Delta H$ | $E_a$ | $\Delta H$ | $E_a$ | $\Delta H$ |
| R1 | CO → C + O | 365.5 | 250.4 | 457.3 | 286.4 | 460.0 | 297.9 | 451.5 | 311.0 |
| R2 | CO + H → CHO | 105.8 | 82.3 | 139.3 | 73.4 | 129.4 | 63.4 | 132.2 | 64.8 |
| R3 | CO + H → COH | 233.3 | 97.8 | 322.2 | 104.6 | 321.9 | 95.3 | 295.6 | 101.1 |
| R4 | CHO → CH + O | 138.2 | −48.4 | 204.2 | 69.5 | 211.4 | 83.8 | 214.4 | 109.3 |
| R5 | CHO + H → CHOH | 89.0 | −3.7 | 109.7 | 10.0 | 111.9 | 11.0 | 127.2 | −11.5 |
| R6 | CHOH → CH + OH | 106.9 | −1.3 | 148.5 | −1.9 | 152.3 | −5.8 | 188.6 | 64.1 |
| R7 | CHO + H → $CH_2O$ | 49.7 | −22.4 | 60.0 | −32.3 | 68.7 | −42.5 | 55.9 | −49.9 |
| R8 | $CH_2O$ → $CH_2$ + O | 111.0 | 29.4 | 203.3 | 85.5 | 213.7 | 79.9 | 213.5 | 118.5 |
| R9 | $CH_2O$ + H → $CH_2OH$ | 89.4 | 3.4 | 107.6 | −1.8 | 112.6 | 1.6 | 105.0 | −13.9 |
| R10 | $CH_2OH$ → $CH_2$ + OH | 84.8 | −19.4 | 124.6 | 12.6 | 130.1 | 13.5 | 167.2 | 83.3 |
| R11 | CHOH + H → $CH_2OH$ | 42.4 | −28.2 | 63.0 | −47.4 | 49.2 | −62.8 | 51.0 | −60.7 |
| R12 | $CH_2O$ + H → $CH_3$ + O | 153.0 | −46.1 | 219.9 | −15.1 | 256.9 | −16.5 | 240.2 | −13.7 |
| R13 | $CH_2O$ + H → $CH_3O$ | 34.7 | −87.6 | 99.2 | −73.5 | 92.7 | −84.0 | 94.0 | −101.7 |
| R14 | $CH_3O$ → $CH_3$ + O | 173.3 | 43.3 | 201.8 | 62.5 | 201.9 | 65.8 | 246.3 | 98.4 |
| R15 | $CH_3O$ + H → $CH_3$ + OH | 185.8 | −4.1 | 289.5 | −10.1 | 303.5 | −6.8 | 308.9 | 19.2 |
| R16 | $CH_2OH$ + H → $CH_3$ + OH | 89.8 | −103.3 | 117.6 | −78.1 | 123.7 | −79.5 | 127.0 | −53.9 |
| R17 | $CH_2$ + H → $CH_3$ | 45.0 | −74.0 | 66.2 | −91.7 | – | – | – | – |
| R18 | $CH_2$ → CH + H | 94.1 | 58.6 | 128.8 | 62.2 | – | – | – | – |
| R19 | $CH_3$ → $CH_2$ + H | 119.0 | 74.0 | 160.5 | 87.0 | 157.6 | 90.7 | 174.6 | 116.0 |

[a] Ref. [30].

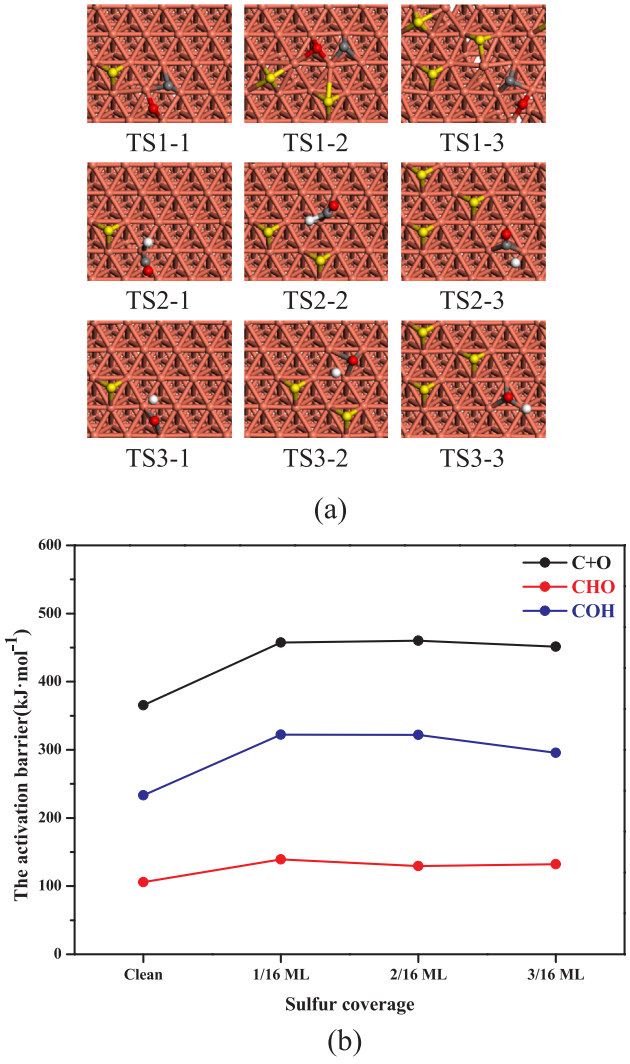


**Fig. 4.** The (a) transition states and (b) variation of activation barriers for CO dissociation and hydrogenation at different sulfur coverage.

Cu(1 1 1) surfaces are all about 460.0 kJ·mol$^{-1}$ which are higher than the value on clean Cu(1 1 1) surface. For CO and H co-adsorbed at different sulfur coverage, CHO is formed through the transition states TS2-1, TS2-2 and TS2-3. In these transition states, the distances between C and H atoms are 1.519, 1.531 and 1.537 Å, respectively, which are longer than that of the C-H distance on clean Cu(1 1 1) surface (1.14 Å). It is worth noting that the C-H distance is increased along with the increment of sulfur coverage, however, the variation of C-H distance is a little on sulfur covered surfaces. The activation barriers of these reactions are 139.3, 129.4 and 132.2 kJ·mol$^{-1}$ at 1/16, 2/16 and 3/16 ML, respectively. While for COH formation, it goes through the transition states TS3-1, TS3-2 and TS3-3 and needs to overcome the activation barriers of 322.2, 321.9 and 295.6 kJ·mol$^{-1}$. In TS3-1, TS3-2 and TS3-3, the lengths between O and H atoms are 1.643, 1.617 and 1.679 Å, respectively.

As shown in Fig. 4(b), the variation of activation barriers for CO dissociation and hydrogenation on sulfur covered Cu(1 1 1) is provided. From the activation barriers of CO dissociation and hydrogenation, the presence of sulfur atoms significantly inhibits the activation of CO, but the variety of the activation barriers is not obvious with the increase of sulfur coverage. Moreover, no matter what the sulfur coverage is, CHO formation is easier than COH formation and CO direct dissociation, which shows that the adsorbed CO species is dominantly hydrogenated to form CHO on sulfur covered Cu(1 1 1) surfaces as that on clean Cu (1 1 1).

Based on the results that CHO is the main product for the activation of CO on sulfur covered Cu(1 1 1) surfaces, beginning with the initial state CHO or CHO + H, the effect of sulfur on $CH_x$($x$ = 1–3) formation were studied.

### 3.2.2. CH formation

Beginning with CHO or CHO + H, our previous results show that there are two possible reaction pathways for CH formation which are focused on the three elementary reactions (R4-R6) [30]. Table 1 and Fig. 5(a) display the activation barriers and transition states involved in CH formation, respectively. The detailed potential energy profiles are shown in Fig. S2.

For Path1, based on the most stable adsorption of CHO on sulfur covered Cu(1 1 1) surfaces, CHO direct dissociation has been studied at different sulfur coverage. Beginning with CHO, the C—O bond breaking goes through the transition states TS4-1, TS4-2 and TS4-3. The

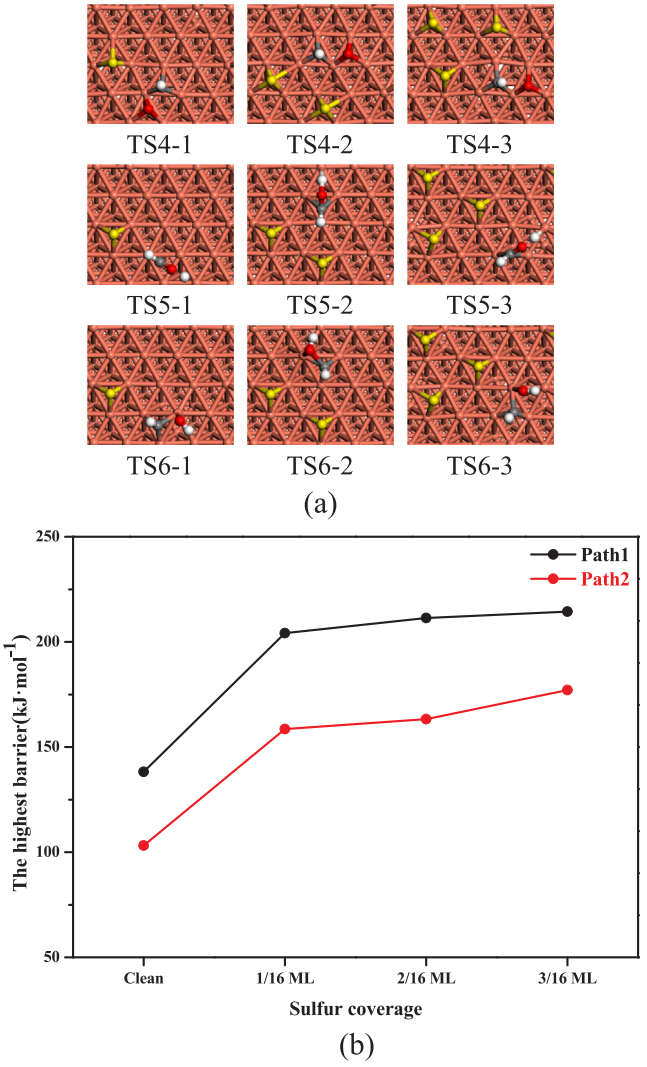


**Fig. 5.** The (a) transition states and (b) variation of the highest barriers for CH formation at different sulfur coverage.

distances of dissociating C—O bond are 1.913, 2.279 and 2.348 Å in these transition states and the processes need to overcome the activation barriers of 204.2, 211.4 and 214.4 kJ·mol$^{-1}$. One can conclude that the activation barriers are higher than that obtained on clean Cu (1 1 1) surface with the value of 138.2 kJ·mol$^{-1}$ [30], and increasing sulfur coverage only causes a small reduction of the activity for CHO direct dissociation. For Path2, CHOH is first formed through CHO hydrogenation and the distances between O and H atoms are 1.420, 1.402 and 1.466 Å in the transition states. These elementary reactions at different sulfur coverage require the activation barriers of 109.7, 111.9 and 127.2 kJ·mol$^{-1}$. After that, the bond cleavage of C—O in CHOH can form CH and OH through TS6-1, TS6-2 and TS6-3. In the transition states, CH binds at the bridge site and the distances of C—O bond are 2.070, 2.041 and 1.988 Å. The elementary reactions have the activation barriers of 148.5, 152.3 and 188.6 kJ·mol$^{-1}$ at different sulfur coverage.

On the basis of the above results, it can be clearly seen that the two reaction pathways for CH formation heavily inhibited after sulfur preadsorbed on Cu(1 1 1) surface (seen in Fig. 5(b)), more importantly, the highest barriers only have a slight change with the increase of sulfur coverage. The highest barriers of the optimal reaction pathways are 158.5, 163.3 and 177.1 kJ·mol$^{-1}$, respectively, which are higher than the value of 103.2 kJ·mol$^{-1}$ obtained on clean Cu(1 1 1) surface [30]. Compared with clean Cu(1 1 1) surface, the possible optimal reaction pathway and rate-limiting step for CH formation on sulfur covered Cu (1 1 1) surfaces still have not changed. The optimal reaction pathway is Path2, in which the rate-limiting step for CH formation at all sulfur coverage occurs at CHOH → CH + OH.

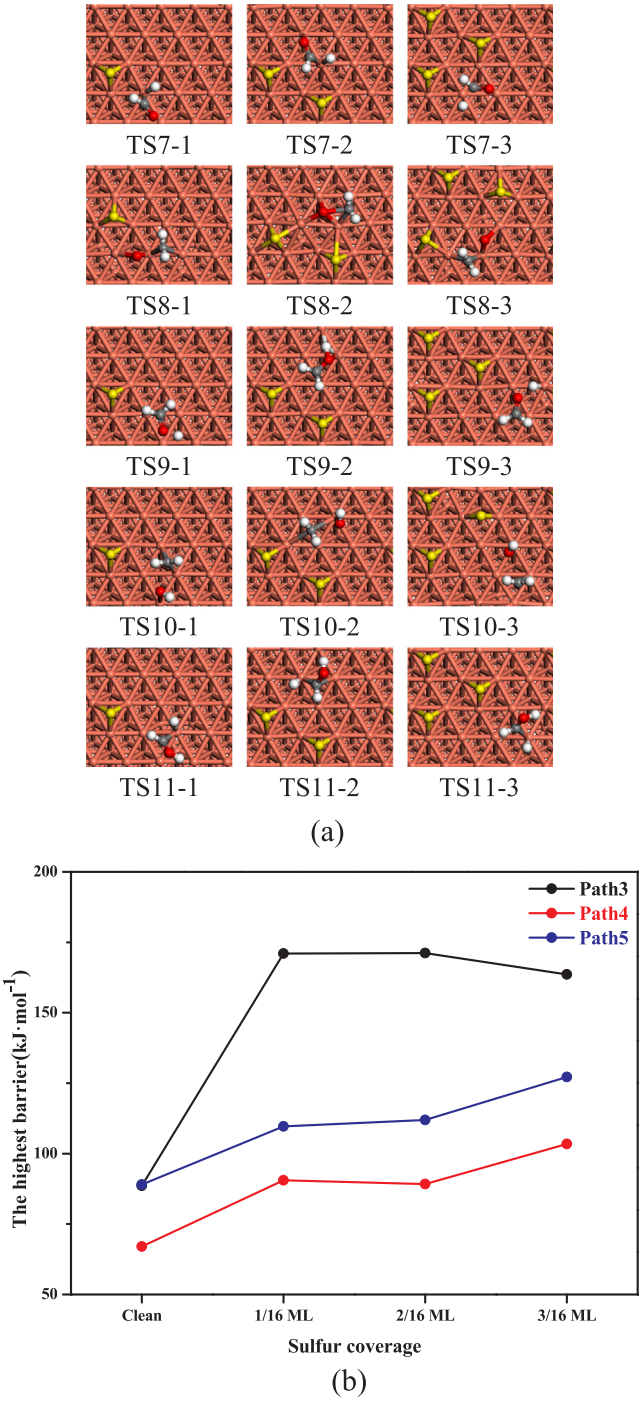


**Fig. 6.** The (a) transition states and (b) variation of the highest barriers for $CH_2$ formation at different sulfur coverage.

### 3.2.3. $CH_2$ formation

Beginning with CHO or CHO + H, here are three possible reaction pathways responsible for the formation of $CH_2$ on Cu(1 1 1) surface [30]. The transition states and activation barriers involved in $CH_2$ formation are provided in Fig. 6(a) and Table 1, respectively. The detailed potential energy profiles are shown in Fig. S3.

For Path3, $CH_2O$ is first formed by CHO hydrogenation via the

transition states TS7-1, TS7-2 and TS7-3. The elementary reactions at different sulfur coverage need to overcome the activation barriers of 60.0, 68.7 and 55.9 kJ·mol$^{-1}$ and the distances of C atom from H atom are 1.689, 1.630 and 1.733 Å in the transition states. After that, the bond breaking of C—O in $CH_2O$ can result in forming $CH_2$ and O through the transition states (TS8-1, TS8-2 and TS8-3) with the activation barriers of 203.3, 213.7 and 213.5 kJ·mol$^{-1}$, and these processes are endothermic by 85.5, 79.9 and 118.5 kJ·mol$^{-1}$, respectively. As for Path4, as mentioned in Path3, $CH_2O$ is first formed by CHO hydrogenation; then, the following step is the hydrogenation of $CH_2O$ to form $CH_2OH$ via the transition state TS9. The activation barriers and reaction energies of the steps occurring at different sulfur coverage are 107.6 and −1.8 kJ·mol$^{-1}$ at 1/16 ML, 112.6 and 1.6 kJ·mol$^{-1}$ at 2/16 ML, 105.0 and −13.9 kJ·mol$^{-1}$ at 3/16 ML. After that, $CH_2OH$ decomposes into the products $CH_2$ and OH via the C—O bond break. The distances of dissociating C—O bond are 2.336, 2.297 and 2.455 Å in the transition states TS10-1, TS10-2 and TS10-3. In these dissociation reactions, the activation barriers of 124.6, 130.1 and 167.2 kJ·mol$^{-1}$ are required to be provided by the system. For Path5, as mentioned in Path2, CHO first hydrogenates to form CHOH; then, starting from CHOH + H, $CH_2OH$ is formed via the transition states TS11-1, TS11-2 and TS11-3. In these transition states, the distances of C atom from H atom are 1.717, 1.723 and 1.717 Å when sulfur coverage increasing from 1/16 to 3/16 ML. The elementary reactions at different sulfur coverage require to overcome the activation barriers of 63.0, 49.2 and 51.0 kJ·mol$^{-1}$ and they are all exothermic by 47.4, 62.8 and 60.7 kJ·mol$^{-1}$, respectively. Further, $CH_2OH$ decomposes into the products $CH_2$ and OH through the C—O bond scission just same as that mentioned in Path4.

On the basis of the above results, we plotted Fig. 6(b) which presents the highest barriers of the three reaction pathways for $CH_2$ formation on sulfur covered Cu(1 1 1). It can be clearly seen that no matter what the sulfur coverage is, the possible main reaction pathway for $CH_2$ formation is not changed. Path4 is still the main route responsible for the formation of $CH_2$, but the rate-limiting steps are changed. In Path4 they are $CH_2OH \rightarrow CH_2 + OH$ at all sulfur coverage, while it is $CH_2O + H \rightarrow CH_2OH$ on clean Cu(1 1 1) surface [30]. The highest barriers of the main reaction pathways are higher than that obtained on clean Cu(1 1 1) surface. In addition, compared Path4 and Path5, the presence of sulfur has the largest impact on Path3. The highest barrier is raised by 80 kJ·mol$^{-1}$ since the appearance of sulfur and remains almost unchanged while sulfur coverage increasing from 1/16 to 3/16 ML.

### 3.2.4. $CH_3$ formation

Beginning with CHO or CHO + H, five possible reaction pathways are responsible for $CH_3$ formation on sulfur covered Cu(1 1 1) surfaces. Table 1 and Fig. 7(a) provide the activation barriers and transition states involved in $CH_3$ formation, respectively. The detailed potential energy profiles are shown in Fig. S4.

For Path6, as mentioned in Path3, $CH_2O$ is firstly formed by CHO hydrogenation; then, the bond breaking of C—O in $CH_2O$ with hydrogen-assisted can result in forming $CH_3$. These elementary reactions go through the transition states (TS12-1, TS12-2 and TS12-3) to form $CH_3$ with the activation barriers of 219.9, 256.9 and 240.2 kJ·mol$^{-1}$ on sulfur covered Cu(1 1 1) when the coverage is 1/16, 2/16 and 3/16 ML, respectively. Correspondingly, the bond lengths of dissociating C—O and forming C—H are 2.109 and 2.300 Å in TS12-1 at 1/16 ML, 2.907 and 2.175 Å in TS12-2 at 2/16 ML, 2.182 and 1.076 Å in TS12-3 at 3/16 ML, respectively. For Path7, based on Path3, the intermediate $CH_2O$ can be hydrogenated to form $CH_3O$ via the transition states TS13-1, TS13-2 and TS13-3. The bond lengths of C atom from H atom are 1.806, 1.878 and 1.891 Å in these transition states. For these hydrogenation reactions, the activation barriers of 99.2, 92.7 and 94.0 kJ·mol$^{-1}$ need provide by the system. Obviously, the presence of sulfur increases the activation barriers of R13 significantly compared with clean Cu(1 1 1) surface of 34.7 kJ·mol$^{-1}$, more importantly, there are little changed

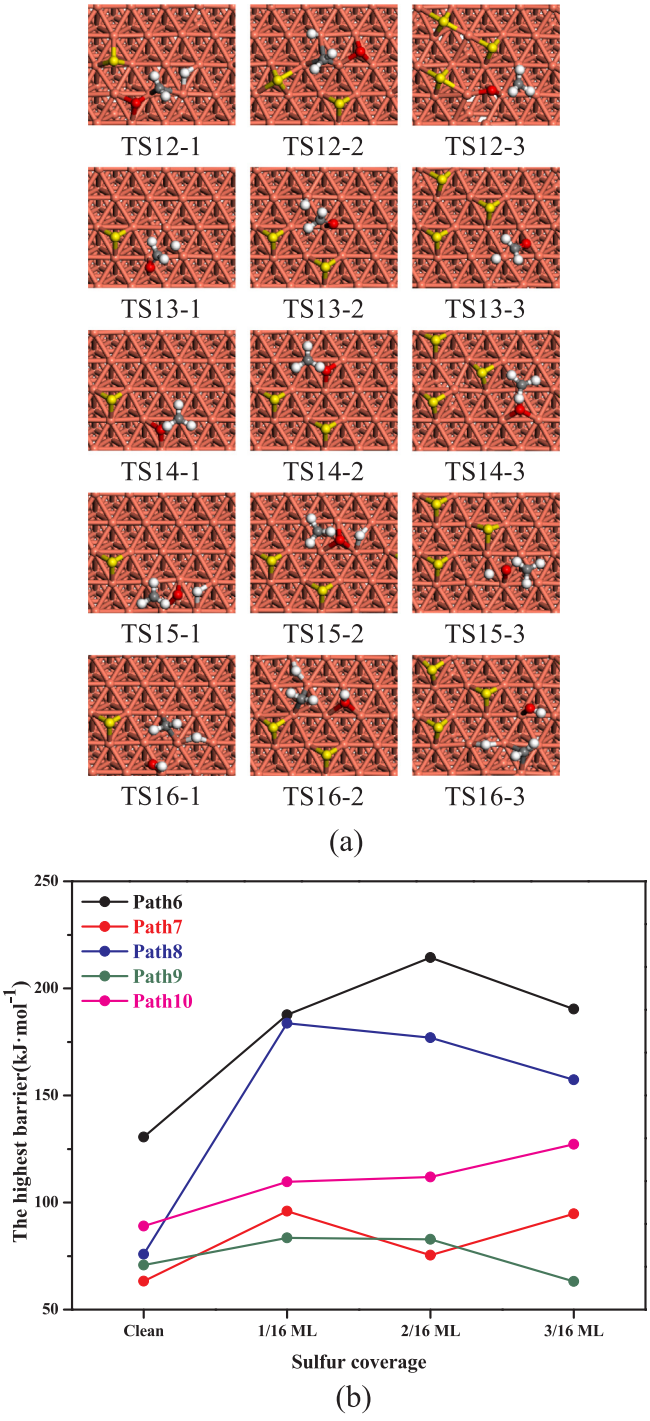


**Fig. 7.** The (a) transition states and (b) variation of the highest barriers for $CH_3$ formation at different sulfur coverage.

when increasing sulfur coverage from 1/16 to 3/16 ML. Then, $CH_3O$ decomposes into the products $CH_3$ and O via the C—O bond break, and the lengths of C—O bond are 2.327, 2.342 and 2.683 Å in the transition states TS14-1, TS14-2 and TS14-3, respectively. These decomposition reactions at different sulfur coverage need the activation barriers of 201.8, 201.9 and 246.3 kJ·mol$^{-1}$. For Path8, as mentioned in Path7, $CH_3O$ is first formed by CHO hydrogenation; then, the following step is the bond breaking of C-O in $CH_3O$ with hydrogen-assisted to form $CH_3$ and OH. The C-O bond lengths are 2.269, 2.291 and 2.156 Å in the transition states (TS15-1, TS15-2 and TS15-3) and the activation barriers of the steps occurring at different sulfur coverage are 289.5, 303.5

and 308.9 kJ·mol$^{-1}$. As for Path9, based on Path4, $CH_2OH$ is firstly formed by CHO hydrogenation; after that, the bond cleavage of C—O in $CH_2OH$ with hydrogen-assisted can lead to $CH_3$ formation through the transition state TS16. These processes at different sulfur coverage have the activation barriers of 117.6, 123.7 and 127.0 kJ·mol$^{-1}$ and they are all found to be exothermic by 78.1, 79.5 and 53.9 kJ·mol$^{-1}$, respectively. For Path10, as mentioned in Path5, $CH_2OH$ is first formed by CHO hydrogenation; finally, the breaking of C—O bond in $CH_2OH$ with hydrogen-assisted can result in forming $CH_3$ and OH, just as described in Path9.

Fig. 7(b) plots the highest barriers of the five reaction pathways for $CH_3$ formation on sulfur covered Cu(1 1 1). It is obvious that the presence of sulfur has some influence on the formation of $CH_3$. According to the highest barriers in Fig. 7(b), the optimal reaction routes for $CH_3$ formation are Path9 at 1/16 and 3/16 ML sulfur coverage, Path7 and Path9 at 2/16 ML sulfur coverage, however, Path7, Path8 and Path9 are the possible main pathways for $CH_3$ formation on clean Cu(1 1 1) surface because of the little difference of highest barriers. Interestingly enough, although the optimal reaction pathways of $CH_3$ formation are changed when sulfur is present in the reaction system, there is no variation in the rate-limiting steps of the five possible pathways. In addition, the highest barriers of all reaction routes for $CH_3$ formation are increased due to the presence of sulfur. The highest barriers of the optimal reaction pathways are higher than that on clean Cu(1 1 1) except at 3/16 ML sulfur coverage.

### 3.2.5. Favorable $CH_x$($x$ = 1–3) monomer

The dominant $CH_x$($x$ = 1–3) species are obtained at different sulfur coverage based on the highest barriers of the optimal reaction routes. As plotted in Fig. 8, at 1/16 ML sulfur coverage, the highest barriers of the optimal reaction routes for CH, $CH_2$ and $CH_3$ formation are 158.5, 90.5 and 83.5 kJ·mol$^{-1}$. Hence, $CH_2$ and $CH_3$ are the dominant $CH_x$($x$ = 1–3) species, which are consistent with those on clean Cu (1 1 1) [30]. However, the dominant $CH_x$($x$ = 1–3) species are only $CH_3$ when increasing sulfur coverage up to 2/16 and 3/16 ML, indicating that the dominant $CH_x$($x$ = 1–3) species are changed from $CH_2$ and $CH_3$ to $CH_3$ under the influence of sulfur. Except for Path9, the highest barriers of possible reaction pathways for $CH_x$($x$ = 1–3) formation are all raised on sulfur covered Cu(1 1 1) surfaces, but an interesting phenomenon is that there are a little changed for CH and $CH_2$ formation when increasing sulfur coverage from 1/16 to 3/16 ML.

Fig. 9 presents the potential energy profile for hydrogenation and dissociation of the dominant $CH_x$($x$ = 1–3) species together with the transition states at different sulfur coverage. The detailed structures of reactants, transition states and products are shown in Fig. S5. At 1/16 ML sulfur coverage, $CH_2$ hydrogenation is easier than other related

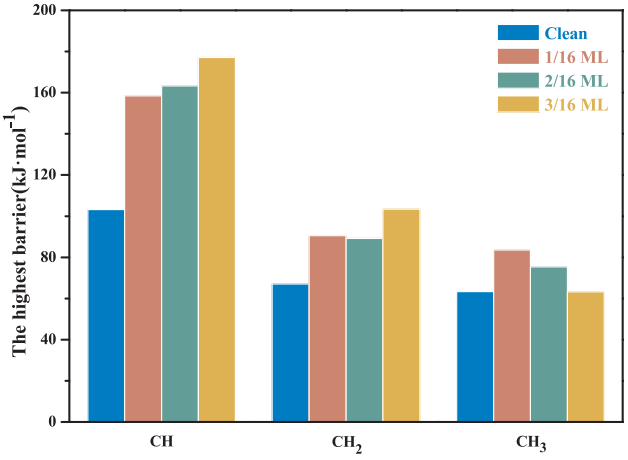


**Fig. 8.** The highest barriers of the optimal reaction routes for CH, $CH_2$ and $CH_3$ formation at different sulfur coverage.

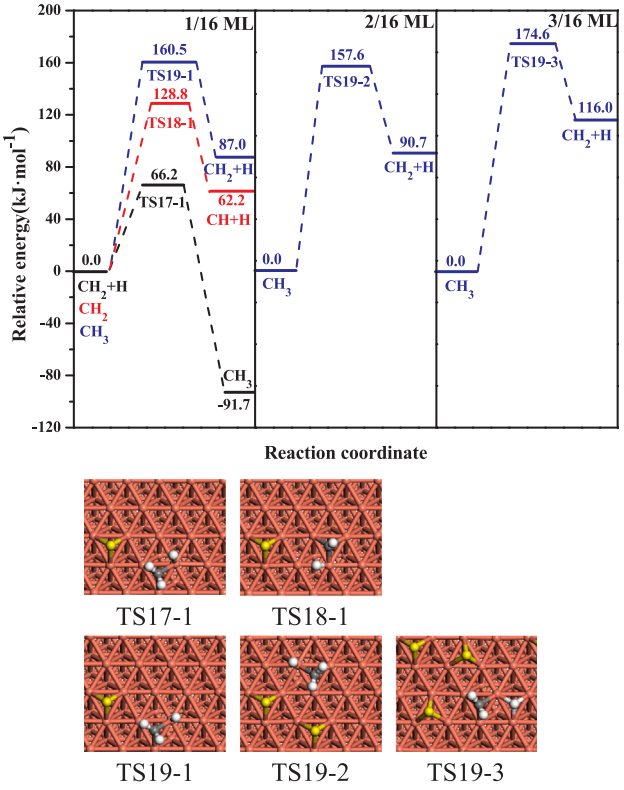


**Fig. 9.** The potential energy profile for hydrogenation and dissociation of the dominant $CH_x$($x$ = 1–3) species together with the transition states at different sulfur coverage.

reactions, which has the activation barrier of 66.2 kJ·mol$^{-1}$ required to be overcome. The dissociation reactions of $CH_3$ at different sulfur coverage have the activation barriers of 160.5, 157.6 and 174.6 kJ·mol$^{-1}$, respectively, which are higher than that on clean Cu (1 1 1) with a value of 119.0 kJ·mol$^{-1}$. Meanwhile, it can be found that the dissociation of $CH_3$ heavily inhibited after sulfur pre-adsorbed on Cu(1 1 1) compared to that on clean surface, but there is only a slight variation with the increasing of sulfur coverage.

### 3.2.6. Summary

Based on the above calculation results, it can be found that the presence of sulfur has influence on the mechanism of $CH_x$($x$ = 1–3) formation, especially for $CH_3$ formation. CO is mainly hydrogenated to form CHO on sulfur covered Cu(1 1 1) surfaces as on clean Cu(1 1 1). Starting from CHO or CHO + H, the optimal reaction pathways for CH and $CH_2$ formation are not changed at all sulfur coverage compared with clean Cu(1 1 1), and the rate-limiting steps for CH formation are also not changed. But the rate-limiting steps for $CH_2$ formation are $CH_2OH \rightarrow CH_2 + OH$ and $CH_2O + H \rightarrow CH_2OH$ in the presence and absence of sulfur, respectively. As for $CH_3$ formation, although the optimal reaction pathways are related to sulfur coverage, the rate-limiting steps of each reaction pathway still remain unchanged whether or not sulfur exists. With sulfur increasing in the reaction system, the dominant $CH_x$($x$ = 1–3) species are changed from $CH_2$ and $CH_3$ at 1/16 ML sulfur coverage to $CH_3$ at 2/16 and 3/16 ML sulfur coverage.

### 3.3. Geometric and electronic structures analysis

In order to investigate the reasons for the change of adsorption energy, we have analyzed the surface geometric structures for each sulfur coverage, but the analysis reveals an unexpected result which is shown in Fig. 10. The lengths of Cu—Cu bond of the most stable adsorption site at 1/16 and 2/16 ML sulfur coverage are shorter than that

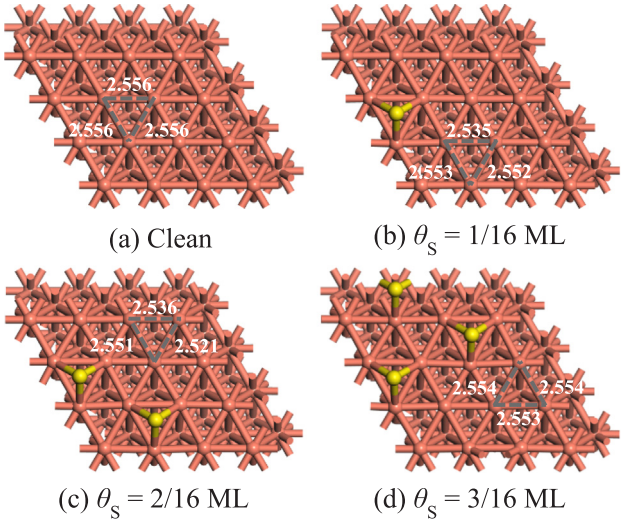


**Fig. 10.** Distortion induced by sulfur adsorption on Cu(1 1 1) surface. Bond lengths are in Å.

**Table 2**
The amount of electrons ($\Delta q/e$) transferred from Cu surface to C, CO and CHOH.

| Species | Sulfur coverage ($\theta_S$) | | | |
|---|---|---|---|---|
| | Clean | 1/16 ML | 2/16 ML | 3/16 ML |
| C | −0.392 | −0.403 | −0.424 | −0.569 |
| CO | −0.326 | −0.335 | −0.359 | −0.387 |
| CHOH | −0.382 | −0.398 | −0.423 | −0.475 |

For $\Delta q$, the "+" and "-" denote surface species gain and lose electrons, respectively.

on clean Cu(1 1 1), oddly enough, it almost has no change at 3/16 ML. Similar phenomenon has been reported in previous study [25] which was found the non-monotonous variation between the metal-metal distances and low sulfur coverage. Apart from geometric analysis, some representative surface species C, CO and CHOH were selected for the Mulliken charge analysis, as listed in Table 2. It can be observed that the number of charge transferred from CHOH to Cu surfaces has an increasing trend with the increase of sulfur coverage, and the result described above can explain the variation of the adsorption energies for CHOH at different sulfur coverage. Normally, the strength of the interaction between adsorbate and substrate is related to charge transfer. The adsorption energies of C or CO on sulfur covered Cu(1 1 1) surfaces exhibit a decreasing trend, while the number of charge transferred from C or CO to Cu surfaces show an increasing trend. It is worth noting that the adsorption strength is not only dependent on charge transfer, but also affected by adsorbates, adsorption sites and direction of charge transfer [50]. For example, Wang and co-workers [51] reported that the adsorption strength of sulfur species on Pt(1 1 1) was the order in S > SH > $H_2S$ even if the number of charge transferred from sulfur species to metal surface was the exact opposite order in $H_2S$ > SH > S.

In spite of this, it is still impossible to explain why a single sulfur atom causes dramatic changes in the adsorption energies of surface species involved in $CH_x$($x$ = 1–3) formation, but there are no significant changes with the increase of sulfur coverage. So what are the main reasons for the changes of adsorption energy at different sulfur coverage will be investigated and discussed in our next work.

## 4. Conclusion

The effect of sulfur on $CH_x$($x$ = 1–3) formation from CO hydrogenation has been investigated using DFT calculations on Cu(1 1 1). The adsorption energies of most surface species are heavily reduced after a sulfur atom pre-adsorbed on Cu(1 1 1) surface compared with those on clean Cu(1 1 1), and the variation of the adsorption energies is little when sulfur coverage increases up to 2/16 and 3/16 ML. In addition, CO is mainly hydrogenated to form CHO whether or not sulfur exists on Cu(1 1 1). Starting from CHO, the optimal reaction routes for CH and $CH_2$ formation are not changed at all sulfur coverage compared with clean Cu(1 1 1), while they are related to sulfur coverage for $CH_3$ formation. With sulfur increasing in the reaction system, the dominant $CH_x$($x$ = 1–3) species are changed from $CH_2$ and $CH_3$ at 1/16 ML sulfur coverage to $CH_3$ at 2/16 and 3/16 ML sulfur coverage. This work provides an insight for understanding the effect of pre-adsorbed sulfur on $CH_x$($x$ = 1–3) formation from synthesis gas reaction over Cu(1 1 1) surface.

## 5. Author contributions section

Theoretical calculations were performed by Huan Lian with assistance of Hongyan Liu, Riguang Zhang, Lixia Ling and Baojun Wang. Hongyan liu and Huan Lian analysed the calculated data together. The project was supervised by Hongyan Liu and Baojun Wang. All authors discussed the results and contributed to the manuscript.

## Declaration of Competing Interest

We declare that we have no financial and personal relationships with other people or organizations that can inappropriately influence our work, there is no professional or other personal interest of any nature or kind in any product, service and/or company that could be construed as influencing the position presented in, or the review of, the manuscript entitled.

## Acknowledgement

This work is financially supported by the Key projects of National Natural Science Foundation of China (No. 21736007), the National Natural Science Foundation of China (No. 21776193, 21576178), Fund Program for the Scientific Activities of Selected Returned Overseas Professionals in Shanxi Province, and Innovation & Application Engineering Research Center For Mesoporous Materials of Shanxi Provice (MMIA2019102).

## Appendix A. Supplementary material

The detailed potential energy profiles for CO activation and $CH_x$($x$ = 1–3) formation together with the related structures on sulfur covered Cu(1 1 1) surfaces are presented. Supplementary data to this article can be found online at https://doi.org/10.1016/j.apsusc.2020.145246.

## References

[1] J.A. Rodriguez, A. Maiti, Adsorption and decomposition of $H_2S$ on MgO(100), NiMgO(100), and ZnO(0001) surfaces: a first-principles density functional study, J. Phys. Chem. B 104 (2000) 3630–3638.
[2] C.H. Bartholomew, Mechanisms of catalyst deactivation, Appl. Catal. A Gen. 212 (2001) 17–60.
[3] A. Bitsch-Larsen, N.J. Degenstein, L.D. Schmidt, Effect of sulfur in catalytic partial oxidation of methane over Rh-Ce coated foam monoliths, Appl. Catal. B Environ. 78 (2008) 364–370.
[4] S. Cimino, L. Lisi, Impact of sulfur poisoning on the catalytic partial oxidation of methane on rhodium-based catalysts, Ind. Eng. Chem. Res. 51 (2012) 7459–7466.
[5] B. Legras, V.V. Ordomsky, C. Dujardin, M. Virginie, A.Y. Khodakov, Impact and detailed action of sulfur in syngas on methane synthesis on Ni/γ-$Al_2O_3$ catalyst, ACS Catal. 4 (2014) 2785–2791.
[6] D.W. Goodman, M. Kiskinova, Chemisorption and reactivity studies of $H_2$ and CO on sulfided Ni(100), Surf. Sci. 105 (1981) L265–L270.
[7] C.T. Campbell, B.E. Koel, $H_2S$/Cu(111): a model study of sulfur poisoning of water-gas shift catalysts, Surf. Sci. 183 (1987) 100–112.
[8] D.E. Jiang, E.A. Carter, Adsorption, diffusion, and dissociation of $H_2S$ on Fe(100)

from first principles, J. Phys. Chem. B 108 (2004) 19140–19145.
[9] S.H. Chen, S.Q. Sun, B.J. Lian, Y.F. Ma, Y.G. Yan, S.Q. Hu, The adsorption and dissociation of $H_2S$ on Cu (100) surface: a DFT study, Surf. Sci. 620 (2014) 51–58.
[10] C.M. Lousada, A.J. Johansson, P.A. Korzhavyi, Molecular and dissociative adsorption of water and hydrogen sulfide at perfect and defective Cu(110) surfaces, Phys. Chem. Chem. Phys. 19 (2017) 8111–8120.
[11] Y.M. Choi, C. Compson, M.C. Lin, M. Liu, A mechanistic study of $H_2S$ decomposition on Ni- and Cu-based anode surfaces in a solid oxide fuel cell, Chem. Phys. Lett. 421 (2006) 179–183.
[12] P.N. Abufager, P.G. Lustemberg, C. Crespos, H.F. Busnengo, DFT study of dissociative adsorption of hydrogen sulfide on Cu(111) and Au(111), Langmuir 24 (2008) 14022–14026.
[13] D.R. Alfonso, First-principles studies of $H_2S$ adsorption and dissociation on metal surfaces, Surf. Sci. 602 (2008) 2758–2768.
[14] M.P. Hyman, B.T. Loveless, J.W. Medlin, A density functional theory study of $H_2S$ decomposition on the (111) surfaces of model Pd-alloys, Surf. Sci. 601 (2007) 5382–5393.
[15] D.R. Alfonso, A.V. Cugini, D.C. Sorescu, Adsorption and decomposition of $H_2S$ on Pd (111) surface: a first-principles study, Catal. Today 99 (2005) 315–322.
[16] O.I. Malyi, K. Bai, V.V. Kulish, P. Wu, Z. Chen, Density functional theory study of sulfur tolerance of copper: new copper-sulfur phase diagram, Chem. Phys. Lett. 533 (2012) 20–24.
[17] S.W. Johnson, R.J. Madix, Modifications of the surface reactivity of Ni(100) by structured overlayers of sulfur: selectivity changes for ethanol and isopropanol decomposition, Surf. Sci. 115 (1982) 61–78.
[18] W.M. Kong, X.L. Zhang, J.J. Mao, X.P. Xu, Y.X. Zhang, Z.X. Yang, Density functional study on the resistance to sulfur poisoning of $Pt_x$(x = 0, 1, 4 and 8) modified α-$Mo_2C$(0001) surfaces, Phys. Chem. Chem. Phys. 19 (2017) 24879–24885.
[19] S.H. Ma, Z.Y. Jiao, T.X. Wang, X.T. Zu, Effect of preadsorbed S on the adsorption of CO on Co(0001), J. Phys. Chem. C 113 (2009) 16210–16215.
[20] J.A. Rodriguez, J. Dvorak, T. Jirsak, G. Liu, J. Hrbek, Y. Aray, C. González, Coverage effects and the nature of the metal-sulfur bond in S/Au(111): high-resolution photoemission and density-functional studies, J. Am. Chem. Soc. 125 (2003) 276–285.
[21] S.H. Ma, Z.Y. Jiao, Z.X. Yang, Coverage effects on the adsorption of sulfur on Co (0001): a DFT study, Surf. Sci. 604 (2010) 817–823.
[22] M.J.S. Spencer, I.K. Snook, I. Yarovsky, Coverage-dependent adsorption of atomic sulfur on Fe(110): a DFT study, J. Phys. Chem. B 109 (2005) 9604–9612.
[23] J.A. Rodriguez, J. Hrbek, M. Kuhn, T. Jirsak, S. Chaturvedi, A. Maiti, Interaction of sulfur with Pt(111) and Sn/Pt(111): effects of coverage and metal-metal bonding on reactivity toward sulfur, J. Chem. Phys. 113 (2000) 11284–11292.
[24] X. Hu, Q. Lu, Y.Q. Sun, J.M. Zhang, Mechanism of trace element adsorption on a clean and S precoated Pd(111) surface: insight from density functional theory calculations, Fuel 107 (2013) 290–298.
[25] M. May, S. Gonzalez, F. Illas, A systematic density functional study of ordered sulfur overlayers on Cu(111) and Ag(111): influence of the adsorbate coverage, Surf. Sci. 602 (2008) 906–913.
[26] R.G. Zhang, G.R. Wang, B.J. Wang, Insights into the mechanism of ethanol formation from syngas on Cu and an expanded prediction of improved Cu-based catalyst, J. Catal. 305 (2013) 238–255.
[27] Z.J. Zuo, L. Wang, L.M. Yu, P.D. Han, W. Huang, Experimental and theoretical studies of ethanol synthesis from syngas over CuZnAl catalysts without other promoters, J. Phys. Chem. C 118 (2014) 12890–12898.
[28] Z.J. Zuo, L. Wang, Y.J. Liu, W. Huang, The effect of CuO-ZnO-$Al_2O_3$ catalyst structure on the ethanol synthesis from syngas, Catal. Commun. 34 (2013) 69–72.
[29] M.V. Twigg, M.S. Spencer, Deactivation of copper metal catalysts for methanol decomposition, methanol steam reforming and methanol synthesis, Top. Catal. 22 (2003) 191–203.
[30] X.C. Sun, R.G. Zhang, B.J. Wang, Insights into the preference of $CH_x$(x = 1-3) formation from CO hydrogenation on Cu(111) surface, Appl. Surf. Sci. 265 (2013) 720–730.
[31] J. Schumann, A.J. Medford, J.S. Yoo, Z.J. Zhao, P. Bothra, A. Cao, F. Studt, F. Abild-Pedersen, J.K. Nørskov, Selectivity of synthesis gas conversion to $C_{2+}$ oxygenates on fcc(111) transition-metal surfaces, ACS Catal. 8 (2018) 3447–3453.
[32] Y.M. Choi, P. Liu, Mechanism of ethanol synthesis from syngas on Rh(111), J. Am. Chem. Soc. 131 (2009) 13054–13061.
[33] R.G. Zhang, X.C. Sun, B.J. Wang, Insight into the preference mechanism of $CH_x$(x = 1-3) and C-C chain formation involved in $C_2$ oxygenate formation from syngas on the Cu(110) surface, J. Phys. Chem. C 117 (2013) 6594–6606.
[34] L.X. Ling, Q. Wang, R.G. Zhang, D.B. Li, B.J. Wang, Formation of $C_2$ oxygenates and ethanol from syngas on an Fe-decorated Cu-based catalyst: insight into the role of Fe as a promoter, Phys. Chem. Chem. Phys. 19 (2017) 30883–30894.
[35] B. Delley, An all-electron numerical method for solving the local density functional for polyatomic molecules, J. Chem. Phys. 92 (1990) 508–517.
[36] B. Delley, From molecules to solids with the $DMol^3$ approach, J. Chem. Phys. 113 (2000) 7756–7764.
[37] J.P. Perdew, J.A. Chevary, S.H. Vosko, K.A. Jackson, M.R. Pederson, D.J. Singh, C. Fiolhais, Atoms, molecules, solids, and surfaces: applications of the generalized gradient approximation for exchange and correlation, Phys. Rev. B 46 (1992) 6671–6687.
[38] J.P. Perdew, K. Burke, M. Ernzerhof, Generalized gradient approximation made simple, Phys. Rev. Lett. 77 (1996) 3865–3868.
[39] M. Dolg, U. Wedig, H. Stoll, H. Preuss, Energy-adjusted ab initio pseudopotentials for the first row transition elements, J. Chem. Phys. 86 (1987) 866–872.
[40] A. Bergner, M. Dolg, W. Küchle, H. Stoll, H. Preuß, Ab initio energy-adjusted pseudopotentials for elements of groups 13–17, Mol. Phys. 80 (1993) 1431–1441.
[41] N. Govind, M. Petersen, G. Fitzgerald, D. King-Smith, J. Andzelm, A generalized synchronous transit method for transition state location, Comp. Mater. Sci. 28 (2003) 250–258.
[42] L.C. Grabow, M. Mavrikakis, Mechanism of methanol synthesis on Cu through $CO_2$ and CO hydrogenation, Acs Catal. 1 (2011) 365–384.
[43] J. Greeley, M. Mavrikakis, Methanol decomposition on Cu(111): a DFT study, J. Catal. 208 (2002) 291–300.
[44] K. Li, C.Z. He, M.G. Jiao, Y. Wang, Z.J. Wu, A first-principles study on the role of hydrogen in early stage of graphene growth during the $CH_4$ dissociation on Cu(111) and Ni(111) surfaces, Carbon 74 (2014) 255–265.
[45] M. Saavedra-Torres, F. Tielens, J.C. Santos, Dibenzyl disulfide adsorption on Cu (111) surface: a DFT study, Theor. Chem. Acc. 135 (2016) 7.
[46] L.Q. Xue, X.Y. Pang, G.C. Wang, Is the preadsorbed sulfur atom always acting as a poison for the surface reaction? J. Phys. Chem. C 111 (2007) 2223–2228.
[47] D.R. Alfonso, A.V. Cugini, D.S. Sholl, Density functional theory studies of sulfur binding on Pd, Cu and Ag and their alloys, Surf. Sci. 546 (2003) 12–26.
[48] D. Curulla-Ferré, A. Govender, T.C. Bromfield, J.W.H. Niemantsverdriet, A DFT study of the adsorption and dissociation of CO on sulfur-precovered Fe(100), J. Phys. Chem. B 110 (2006) 13897–13904.
[49] L.Y. Gan, Y.X. Zhang, Y.J. Zhao, Comparison of S poisoning effects on CO adsorption on Pd, Au, and bimetallic PdAu(111) surfaces, J. Phys. Chem. C 114 (2010) 996–1003.
[50] J. Sivek, H. Sahin, B. Partoens, F.M. Peeters, Adsorption and absorption of boron, nitrogen, aluminum, and phosphorus on silicene: stability and electronic and phonon properties, Phys. Rev. B 87 (2013) 085444.
[51] H.Z. Wang, W. Zhang, J.W. Jiang, Z.J. Sui, Y.A. Zhu, G.H. Ye, D. Chen, X.G. Zhou, W.K. Yuan, The role of $H_2S$ addition on $Pt/Al_2O_3$ catalyzed propane dehydrogenation: a mechanistic study, Catal. Sci. Technol. 9 (2019) 867–876.